Effect of a singular planar heterogeneity on tensile failure

Pluymakers, A.M.H.; Bakker, R.R.; Ter Steege, F.B.; Versluis, B.; Barnhoorn, A.

DOI
10.1016/j.ijrmms.2023.105448

Publication date
2023

Document Version
Final published version

Published in
International Journal of Rock Mechanics and Mining Sciences

International Journal of Rock Mechanics & Mining Sciences 170 (2023) 105448

Contents lists available at ScienceDirect

International Journal of Rock Mechanics and Mining Sciences

journal homepage: www.elsevier.com/locate/ijrmms

Effect of a singular planar heterogeneity on tensile failure

A.M.H. Pluymakers *, R.R. Bakker, F.B. Ter Steege, B. Versluis, A. Barnhoorn

Department of Geoscience and Engineering, TU Delft, Stevinweg 1 2628CN Delft, the Netherlands

ARTICLE INFO

Keywords:
Tensile strength
Heterogeneity
Anisotropy
Stylolite
Limestone
Fracture

ABSTRACT

Many rocks contain planar heterogeneities, in the form of open fractures, veins and/or stylolites, but scarce data exist on how strength and fracture pattern formation is affected by the presence of a singular planar heterogeneity in an otherwise uniform matrix. The mechanics of stylolite-bearing and/or fractured limestone is of interest to several engineering applications, from quarries to subsurface gas or geothermal reservoirs. We have performed Brazilian Disc tests on pre-fractured Indiana limestone samples and Treuchtlinger Marmor discs which contain cohesive stylolites, investigating Brazilian test Strength and the resulting fracture pattern. All experiments were filmed, and where possible analyzed with particle image velocimetry. When viewed in 2D, the planar discontinuity was set at different rotation angles compared to the principal loading direction, where perpendicular to the loading direction is defined as 0°. The results show that all samples are weaker than their intact counterparts. For the pre-fractured Indiana limestone, there is 10–75% angle-dependent weakening. However, in the samples with a stylolite, strength is weakened by 35–75%, independent of direction. Several new cracks appeared when fracturing a stylolite-sample, where the orientation is heavily influenced by the stylolite orientation. The fracture pattern and associated stress drops are more complex for high angles. In these samples always more than one fracture formed, whereas in pre-fractured samples usually only one new fracture formed. This suggests a potential for more permeability increase when hydrofracturing a stylolite-rich interval. Comparison with Finite Element Models indicates that this difference in fracture pattern is caused by the strength contrast between the anastomosing stylolite zone and the matrix material, leading to stress concentrations effects. This causes (micro-) fracture nucleation to occur locally, promotes fracture coalescence and fracture growth at lower overall sample-load conditions compared to intact samples.

1. Introduction

In many formations, outcrop and boreholes several singular planes of weakness or heterogeneities are present, in the form of pre-existing fractures, sealed veins and/or stylolites. In rock mechanical testing, samples with such obvious heterogeneities, i.e. including a vein or pre-existing fracture, are usually discarded, since they are not considered to be representative for the bulk strength. However, not all rocks are perfect, and many formations will contain several of such planes, with a variable spacing of millimeters to several meters apart. The presence of such a singular plane of weakness is a specific class of anisotropy, which to date has scarcely been investigated, even though it is of interest to several engineering applications. For example, the (tensile) failure behavior of imperfect limestone is of interest to the natural stone industry and in quarries (c.f., López-Buendía et al.[1] and in subsurface geo-engineering operations, fractures are key. All these projects are either about keeping the fluid where it is (CO_2 or H_2 storage), or about how to get the fluid out. The presence of faults and fractures can strongly affect the flow behavior and thereby production (for example, Knipe et al.[2] for hydrocarbon reservoirs; or Wang et al.[3] for geothermal fractured reservoirs). At larger depths, hydrofracturing is a common method to improve connectivity of reservoirs, for which tensile strength is a key parameter. The ability to predict fracture generation pressure, fracture orientation and the weakest direction, also for imperfect rocks, would therefore allow for an improved quantification of the effectivity of hydraulic fracture, with uses to various forms of geo-energy. Three broad categories of singular planes of weakness exist: open fractures, stylolites and veins.

Despite the frequent occurrence of fractures, veins and stylolites, to date, when testing imperfect samples for their mechanical anisotropy, samples are usually retrieved from laminated anisotropic rocks, i.e. with a set of semi-parallel planes of weakness (i.e. bedding, foliation, etc.). The effect of such anisotropy on tensile strength and the resulting fracture patterns has been under investigation in different studies for

* Corresponding author.
E-mail address: anne.pluymakers@tudelft.nl (A.M.H. Pluymakers).

https://doi.org/10.1016/j.ijrmms.2023.105448
Received 8 February 2022; Received in revised form 2 March 2023; Accepted 30 May 2023
Available online 26 June 2023

decades (e.g. Refs. 4–15). All these studies investigate laminated rocks, i.e. the effect of bedding or foliation in sandstones, shales or metamorphic rocks. The results show that in general the samples with the bedding parallel to the maximum principal stress (high angles) exhibit the lowest strength, and that samples exhibit maximum strength when the bedding is parallel to the minimum principal stress (low angles). The curve of strength as a function of angle shows a gradual transition between these two endmembers, often with a high and steady "shoulder" at high angles, see Fig. 1. Modeling studies have shown failure at high angles is related to tensile failure along the weakness planes; at intermediate angles there is shear failure along the weakness planes, and at low angles it is tensile failure of the intact rock.[11] Absolute strength, but also the location of the shoulder depends on rock type, and presumably on the strength or cohesion of the interface (which in terms of bedding is most likely connected to the deposition and/or burial history[7,12]).

Carbonate formations are frequent hydrocarbon[16] or geothermal reservoir rocks (e.g. Refs. 17,18), for which flow, or the lack thereof, can have important implications for the suitability of a reservoir. Limestone reservoirs are recently in the spotlight for geothermal energy, in particular in the United Kingdom,[19] Netherlands[20,21] and Germany,[18] and many of these reservoirs are karstified and full of stylolites.[21] Therefore, the formation and flow properties of stylolites have been of particular interest to the carbonate-community in the past decade (e.g., see reviews by Toussaint et al.[22] and Bruna et al. [23]). They are considered "anti-mode I cracks", and form through dissolution. In 2D, stylolites are visible as undulating, darker lines, with "teeth" of various amplitude. There are three types: i) bedding-parallel stylolites, which develop during burial; ii) tectonic stylolites, which develop during slip; and iii) slickolites, which exhibit a plane oblique to the displacement direction (Ref. 23 and references therein). For the first two types, teeth develop parallel to the maximum principal stress.

Different stylolite types exist, with different flow properties, which are a consequence of their formation history and lithology. Since they are the results of dissolution, it logically follows that they have been fluid conduits at some point.[23] However, since their formation can include the collection of insoluble material such as clay or organic matter (c.f.[24,25]) they have the potential to be a directional-dependent barrier to flow as well. Often there is a (mm-scale) low-porosity zone in the surrounding of the stylolite, though microscale observation show that the porosity in the micrometer vicinity of a stylolite can actually be higher than that of the matrix.[26] Experimental observations confirm that stylolites are indeed not universal barriers to flow.[27]

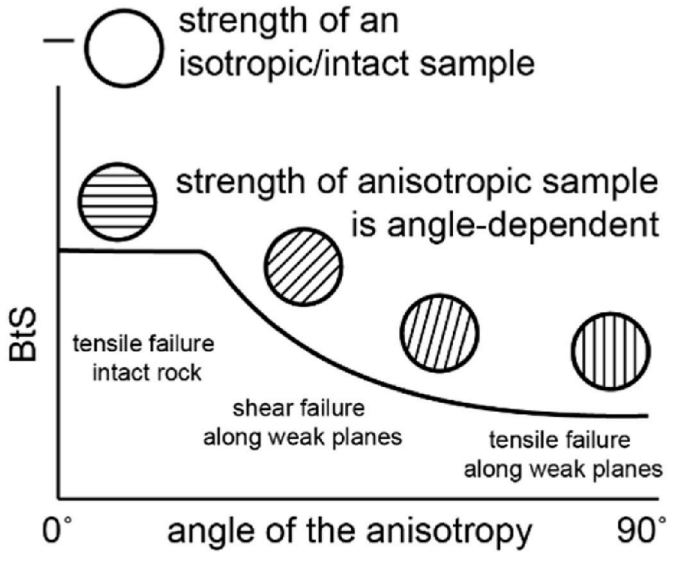

Fig. 1. Schematic of how Brazilian test Strength (BtS) in a layered, anisotropic sample depends on testing angle (after.[11] There is a high and steady BtS at low angles which forms a shoulder, followed by a gradual transition to low BtS at high angles.

Stylolites have been inferred to be planes of weakness, but overall, their mechanical properties are not well characterized. Most mechanical research has focused on their properties as a building material, since stylolite-bearing rocks are regularly used as decorative building material, as slabs or kitchen counters.[1,28,29] In this practical context they are clearly seen as planes of weakness. First tests have shown that in a compressive configuration their strength is anisotropic, with a minimum in strength for oblique angles,[30] which in a more systematic study has been interpreted as an effect of the inferred high porosity zone[31].[31] Baud et al. did not record any mechanical anisotropy for thin and closed stylolites, and they inferred stylolites only become a plane of weakness when they have a certain thickness with an associated thickness of the high porosity band. However, to date, few tensile strength data is available. To our knowledge, the only tensile tests performed on this kind of single plane of weakness are by López-Buendía et al.[1] They have performed tests with the stylolite plane parallel to σ_1, and compared the strength of open stylolite to that of a partially closed and of a cemented stylolite. They have shown that cemented stylolites are stronger than partially open stylolites, which are stronger than fully open stylolites, but they do not provide a measure of the anisotropy of strength, even though the studies on laminated rocks indicate clearly structural anisotropy and mechanical anisotropy are linked.[7,11–13] Moreover, given the high variability in flow properties of stylolites, it seems plausible that the mechanical properties can also differ depending on their exact formation history.

In the following, we will compare the anisotropy of tensile strength, and the resulting fracture patterns, between limestone samples which contain a central singular heterogeneity. Keeping the heterogeneity in the center of the sample is the simplest geometry possible, and the easiest to reproduce. Of the three broad categories of open fractures, stylolites and veins, we decided to focus on a comparison between open fractures and stylolites. Modeling studies show that the strength of veins can be relatively well modeled, since the three controlling factors are the strength of i) the matrix, ii) the vein material and iii) the interface between vein and matrix.[32,33] A stylolite has a complex microstructure and can therefore not be separated in such straightforward zones. The strength of an open fracture will then be determined by the strength of the interface, since there will be matrix strength on both sides and no vein material, i.e. there is no cohesion between both sides. In the following, we investigate how failure proceeds and where new cracks open as a function of angle in the case of a pre-existing open fracture (no cohesion) versus the case of a stylolite, i.e. an interface with unknown but significant cohesion.

2. Method

2.1. Description starting material

2.1.1. Indiana limestone

The Indiana limestone is a calcite-cemented grainstone according to the Dunham classification.[34] All intact samples had a porosity between 17.8 and 20.0% as measured on oven-dry samples with helium-pycnometry. The grains are variable in size between 20 μm up to several mm, with variable shapes, see Fig. 2. These samples are fractured and then the resulting fracture is placed at the desired angle inside the BtS assembly.

2.1.2. Treuchtlinger marmor

The Treuchtlinger Marmor is a mud-supported wackestone.[34] The samples with approximately bedding-parallel stylolites ranged in porosity from 10.6 to 13.4%, with two apparent outliers with a porosity of 15.9 and 17.1%. The homogenous samples without stylolites had a porosity between 6.7 and 20.1%. All porosities are measured on oven-dry samples with helium-pycnometry. We selected samples such

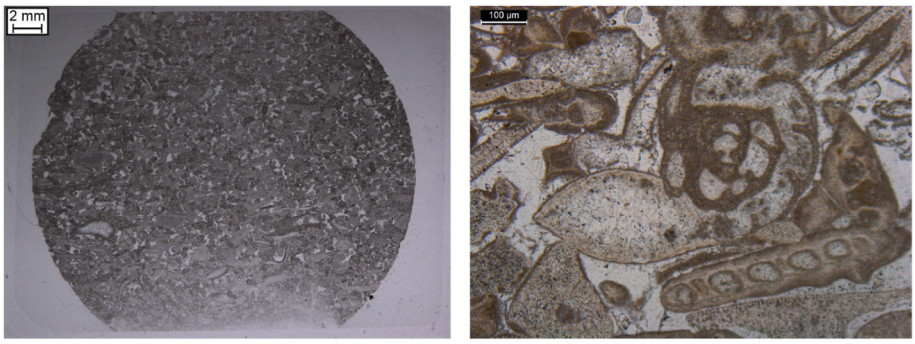

Fig. 2. Plane polarized light images of the Indiana limestone ysed a) Overview and b) detail.

that they contained a central stylolite, where the (roughly planar) stylolite would run diametrically across the sample as much as possible in the available sample batch. This is also why we included the two higher porosity samples. We investigated selected stylolite samples with microtomography (Fig. 3; before failure), by eye (Fig. 4a and b), electron (Fig. 4c–e) and optical microscopy (Fig. 4f). In the microtomography scans, only the porosity is visible, i.e. there are no visible amounts of high density minerals on this voxel resolution of 15 µm. For the 4 CT scans made, in all samples the porosity alongside the sample was crosscutting the entire sample, i.e. there is an open fracture with the same orientation and rough location as the stylolite (see Fig. 3). On a separate sample, we imaged the surface expression of the stylolite using scanning electron microscopy, showing that at the location of the stylolite there is a dip on the surface of several 100 µm depth and width (Fig. 4c–e). Also on this microscale, the stylolite itself has an organically anastomosing geometry. There are undulating strands of micrometer width which retain integrity even when not fully supported by surface grain material (Fig. 3d and e). Optical microscopy under transmitted light, of a separate sample not used for mechanical testing, shows that the stylolite forms a pervasive anastomosing network where all strands vary in width and connectivity (Fig. 4f). Moreover, the stylolite crosscuts and/or connects several carbonate veins with euhedral crystals. Both in plane polarized light and under cross polarized light it appears as light-to dark brown. Throughout the sample there are several irregular, elongated dark brown patches present up to mm length and microns wide. There is no evidence of clay minerals, hence we interpret that the stylolite is an organic- or bitumen-rich zone. Note that several of the wider (up to 400 µm wide) strands of the network are associated with an open crack (aperture on the micrometer-scale; Fig. 4f). This open crack is not continuous: there are several mineral/material bridges. This implies that the crack was already present in-situ in the quarry.

2.2. Procedure

We have performed indirect uniaxial tensile strength tests, commonly referred to as Brazilian Disc tests, on limestone samples using a loading frame with a 50 kN load cell with measurement uncertainty 2 N, equipped with two Linear Vertical Differential Transducers (LVDT) with a 2 mm resolution and a measurement uncertainty of 2 µm. In our setup (Fig. 5), samples are 30 mm in diameter, and about 15 mm in thickness. We used Indiana limestone samples (IL), which we fractured in a standard Brazilian Disc Indirect Tensile Strength test, leading to a standard tensile fracture, and we used Treuchtlinger Marmor samples (TM) (location described in Ref. 35 which contained a central stylolite. For the IL samples, before testing the samples were wrapped with a thin layer of tape to keep both halves together. The tape does not stretch, but only plastically deforms, and reference tests with and without tape on Indiana limestone did not show a significant change in tensile strength. The sample containing a tensile fracture or a stylolite was placed inside the loading frame with variable rotation angle (see Table 1). The rotation angle was defined to be 0° when the fracture or stylolite normal was parallel to the loading direction, and 90° when the fracture or stylolite normal was perpendicular to the loading direction (Fig. 5). Once placed, the samples were fractured again whilst filming one of the surfaces. The chosen displacement rate of 1 µm/s always led to failure within a few minutes, following the ASTM guidelines. The film series were, where possible, analyzed with Particle Image Velocimetry (PIV).

As indicated, the IL samples were used twice: immediately after the first failure (i.e. no sliding allowed) the samples were unloaded, and subsequently rotated to be “fractured” again. This second series was filmed using an iPhone XS. Note that due to lens distortion near the sample (the round disc is not round in the video), these data were not analyzed with PIV. To enable more accurate determination of particle movement, the second series, with TM samples, was filmed with a Digital Single Lens Reflex camera (50 frames/second) with fixed aperture, fixed lighting and exposure settings, to enable tracing of surface motion with PIV.

Note that using the Brazilian Disc test is an indirect measure of tensile strength, which is based on the assumption a homogeneous sample is broken. However, in this case, it is used on a sample with a discontinuity. Therefore, following previous workers,[7,11,36,37] we will label the highest peak in the mechanical results not as tensile strength but as Brazilian test Strength or BtS. For reference purposes, we also fractured 18 intact homogeneous IL samples, to obtain the tensile strength, and 6 intact samples of intact homogeneous TM using the same apparatus and the standard Brazilian Disc Indirect Tensile Strength procedure.[38]

2.3. Particle image velocimetry (PIV)

Particle Image Velocimetry is an image analysis technique which compares displacement of the different features present on images which differ in acquisition time. In this study we use the Matlab-based software tool “PIVlab”.[39] It calculates the velocity distribution within frame-pairs and can be used to derive and display the strain rate as a function of location in the sample. Extension is positive, and compression is negative. We calibrated each image using the known diameter of the samples before fracture (29.5 mm), and calculated the first invariant of the strain rate as $\dot{e} = \frac{\partial u}{\partial x} + \frac{\partial v}{\partial y}$, where u is the horizontal velocity (x-direction, 0°) and v is the vertical velocity (y-direction, 90°).[39] In the PIVlab procedure, we selected only the limestone disc as region of interest. We used the correlation algorithm ‘Fast Fourier Transform window deformation’, and the data was analyzed in three passes. The passes used were 64, 48 and 24 pixels (1 pixel is between 150 and 200 µm, depending on the experiment), which is related to the average aperture and length of the fractures. The displacement information of the first pass is used to offset the interrogation areas in the second pass and so on.[39] The tool uses 50% overlap between sub-windows. When present, singular outliers are discarded manually.

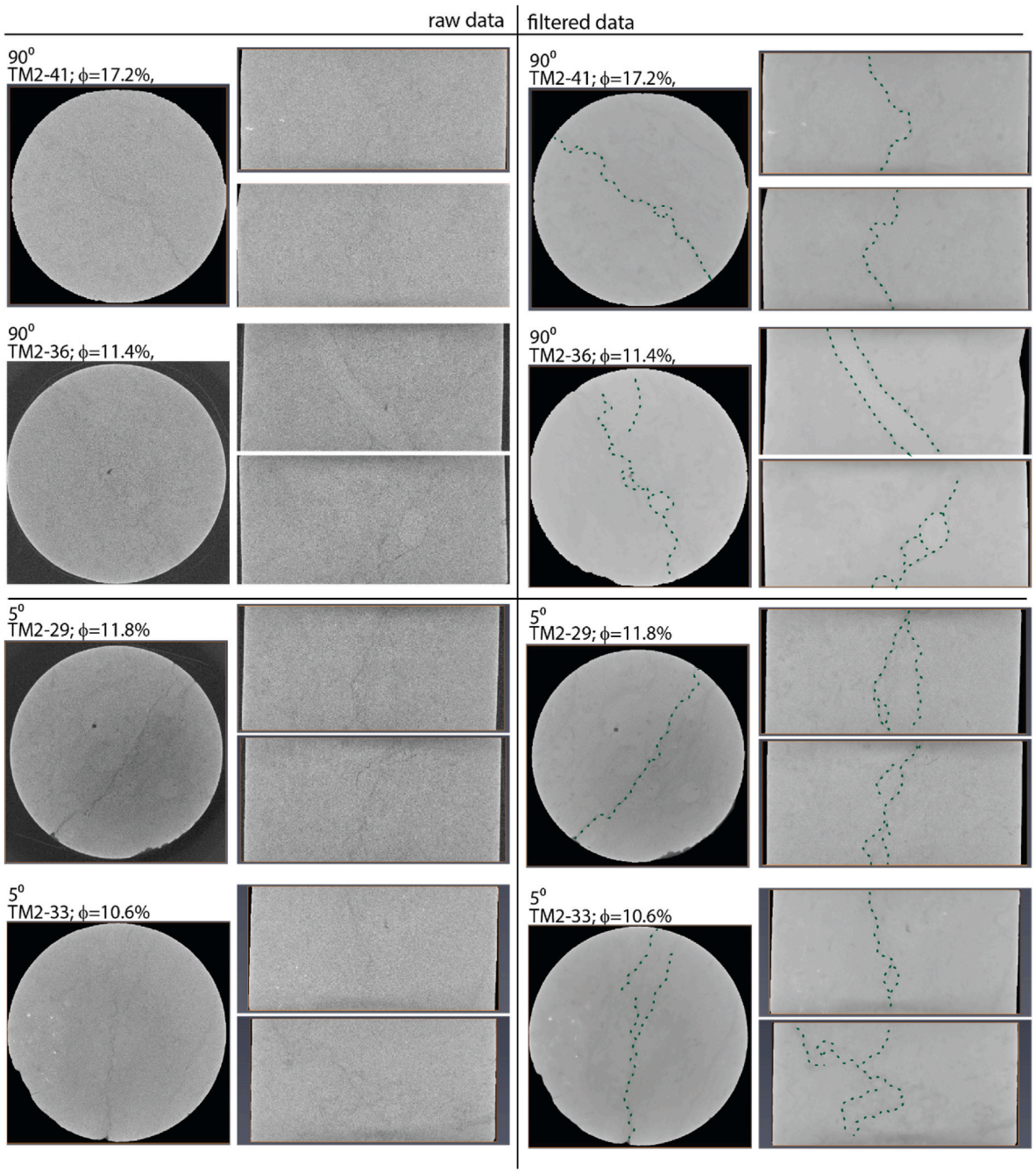

Fig. 3. Microtomography of selected stylolite samples before testing. Left the raw data, and on the right the filtered data (non-local means filter), which highlights the greyscale contrast between porosity (dark), the larger fossils (bright) and the matrix. Superimposed in green dotted lines the porosity associated with the edge of the stylolite. The view is approximately 30 mm wide, with a voxel size of 15 μm. In all samples, there is a semi-continuous, anastomosing band of porosity with a similar orientation as the stylolite, indicating the stylolite is associated with the porosity. The aperture of this open space parallel to the stylolite is variable, and at most 2-3x the voxel size.

2.4. Finite element models

To further illustrate the stress field inside a simulated stylolite sample, the Brazil Disc tests with stylolite have been simulated using the finite element software "COMSOL Multiphysics®". We used a 2D plane strain approach, with the "structural mechanics" COMSOL module.[40] The numerical code calculates the 2D stress field as a result of a point load assuming linear elasticity. This implies that the model only represents the elastic part of the load-time graph from the physical tests. Any events of sudden loss of load carrying capacity are likely the effect of fracturing inside the sample and are not captured by this numerical model. Note that modeling the behavior of fractured samples (including the IL samples) would require a fracture mechanics approach, that would allow for inclusion of crack nucleation and coalescence (e.g., Refs. 41,42), which is beyond the scope of this work. The model results are only used to illustrate the potential effects of stress concentrations due to the presence of an initially cohesive heterogeneity, such as stylolites (or veins), not for open, cohesionless fractures. The results are therefore only used for qualitative interpretation, and any (semi-) quantitative results cannot be 1:1 compared to laboratory results.

Simulated circular cross-sections (30 mm diameter) were subjected to a (stepwise increasing) point load in the direction of the fixed point,

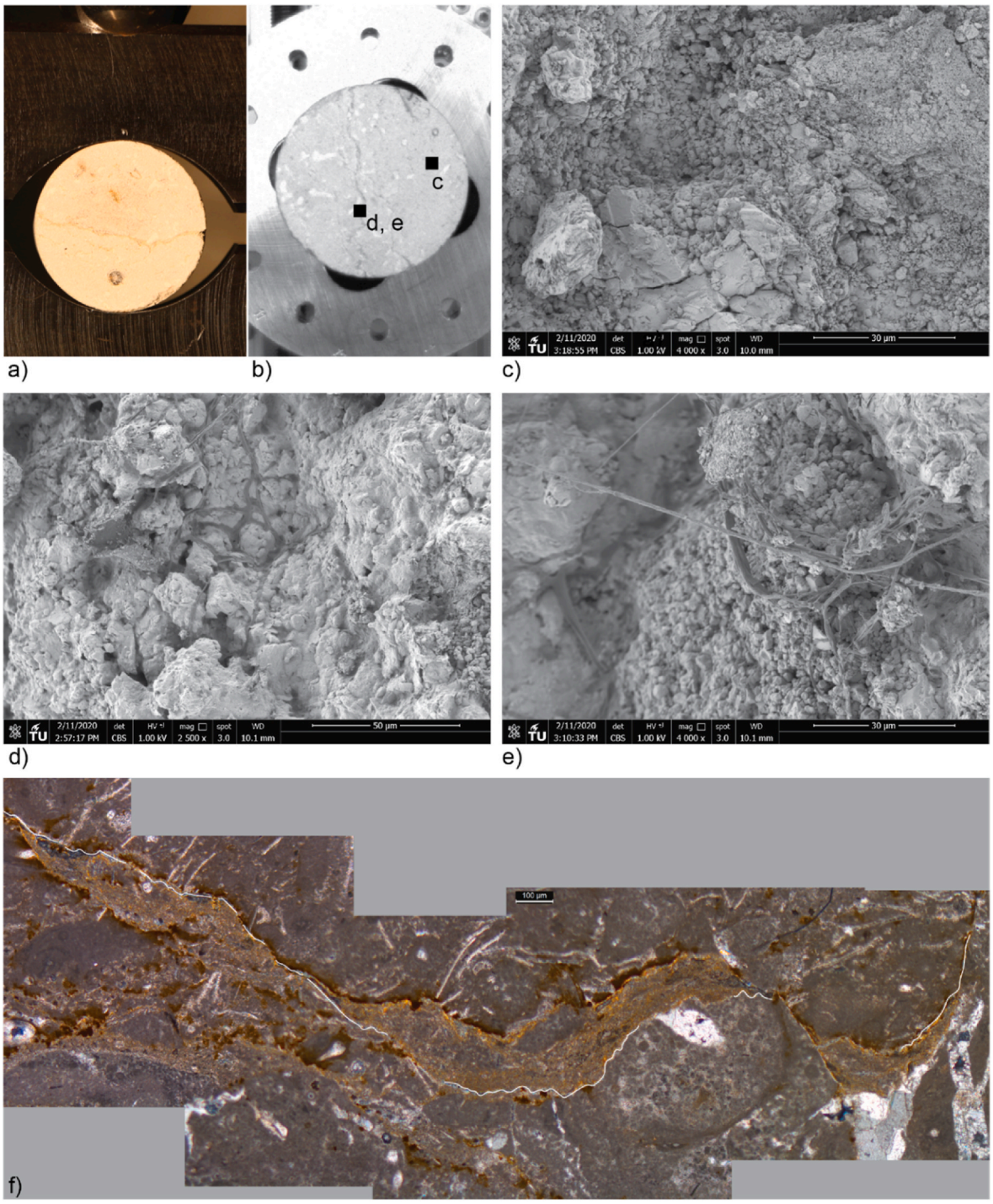

Fig. 4. Stylolite in Treuchtlinger Marmor a) inside the Brazilian Disc assembly and b) inside a Scanning Electron Microscopy (SEM; unpolished, uncoated); b) SEM micrograph, far away from the stylolite and c; d) SEM micrograph of the stylolite itself, which consists out of plastic anastomosing strings, which are more resistant to weather than the carbonate rock surface as is shown in e); f) stitched cross-polarized optical micrograph of one of the main strands of a stylolite in a Treuchtlinger Marmor sample. The porosity band is traced in white; note how it is associated with the edge of the main stylolite and is discontinuous.

diametrically across the sample while other boundaries were free. The geometry of the stylolite is a sine wave with an amplitude of 3 mm, a period of 15 mm (i.e. 2 waves along the sample diameter) and a thickness of 2 mm. The regular sine wave does not necessarily follow the more chaotic nature of the anastomosing stylolite geometry, but is sufficient for our illustrative purpose as well as being reproducible. The simulated sample consists of a host rock with realistic values for limestone: Young's modulus $E = 10$ GPa and Poisson's ratio: $\upsilon = 0.25$. The Young's modulus of the stylolite band is varied ($E = \{100, 20, 10, 5, 1\}$ *GPa*), and the Poisson's ratio is kept the same as the host rock. These finite element models were used to gauge the effect of differing relative strength, as well as simulating how the resulting stress field varies as a function of rotation of the sinusoidal "stylolite".

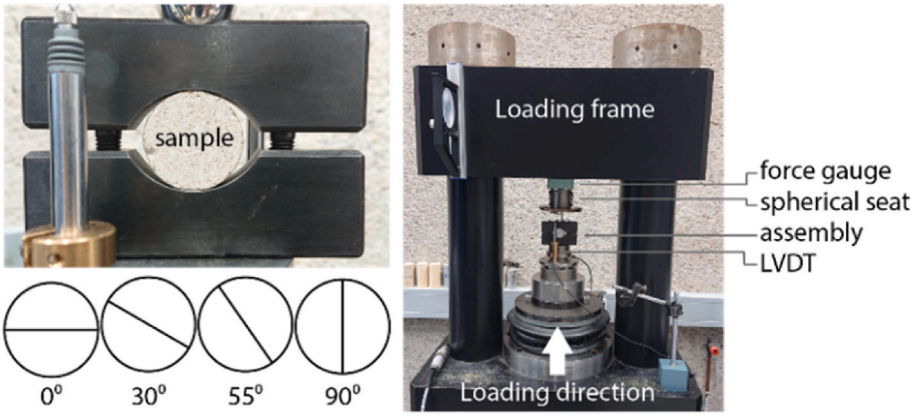

Fig. 5. Photo of sample in Brazilian disc assembly and press, including sketches of the orientations. Samples are 30 mm in diameter.

Table 1
Summary of the experiments on fractured samples and stylolite samples (see Table A1 for details on sample numbers, porosity and BtS for each individual sample).

Rock type	Initial fracture	Angle	Number of experiments
IL	Tensile	20°	1
IL	Tensile	30°	2
IL	Tensile	35°	1
IL	Tensile	37.5°	1
IL	Tensile	40°	1
IL	Tensile	45°	2
IL	Tensile	50°	2
IL	Tensile	60°	2
IL	Tensile	90°	1
TM	Stylolite	0°	2
TM	Stylolite	20°	1
TM	Stylolite	30°	2
TM	Stylolite	45°	2
TM	Stylolite	60°	2
TM	Stylolite	90°	2

3. Results

3.1. Mechanical data

The stress-displacement curves for all tests are given in Appendix Fig. A1, and the Brazilian test Strength as a function of angle in Fig. 6. The maximum peak stress of a stress-displacement plot is the Brazilian test Strength or BtS, which in a homogeneous sample would be equivalent to tensile strength. As can be seen in Fig. 6a, all pre-fractured IL samples are 10–75% weaker than intact samples. The resulting BtS and the amount of weakening are orientation dependent. Overall, the samples with steeper angles are weaker, i.e. when the fracture is oriented parallel to the maximum principal stress. For the stylolite TM samples the samples are all 30–85% weaker than an intact, homogeneous sample without stylolite. These samples are more isotropic in strength, without a clear dependence of strength on direction.

3.2. Image data

For all IL samples, we collect three snapshots of the camera data in Fig. 7. For each experiment, the left image is the starting situation, the middle image is the situation during loading but before failure, and the right image shows the final geometry. For samples with an initially steep angle of 65–70°, no new cracks are initiated. During loading, the original crack remains visible and does not fully close. Once reactivated, deformation occurs by frictional sliding along the original fracture plane. We will refer to these steep-angle samples as type I. The other endmember are samples where the initial crack is close

to horizontal, which we will refer to as type IV. In these samples, the original fracture becomes difficult to distinguish during loading, i.e. the original fracture closes. The new fracture initiates in the orientation that would be expected for intact homogeneous material, i.e. the fracture initiates at the center of the sample and runs diametrically across in the

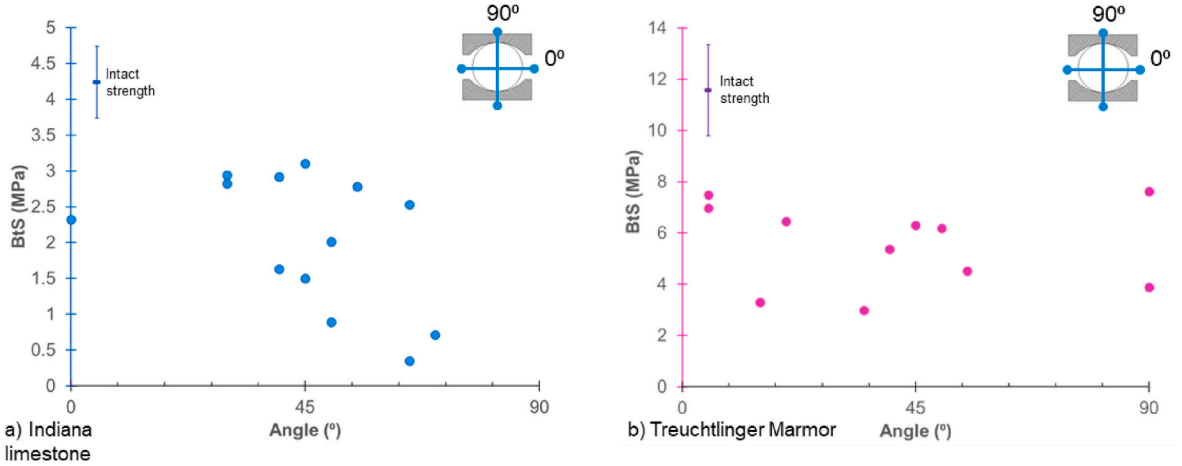

Fig. 6. The maximum strength of each sample as a function of the initial angle; a) for the initially fractured Indiana limestone samples and b) for the Treuchtlinger Marmor samples with the initial stylolite. On the left side of the diagrams (at 5°) is the initial sample strength and the standard deviation, which for Indiana limestone is the average of 20 samples, and for Treuchtlinger Marmor the average of 6 samples. Measurement error is below symbol size.

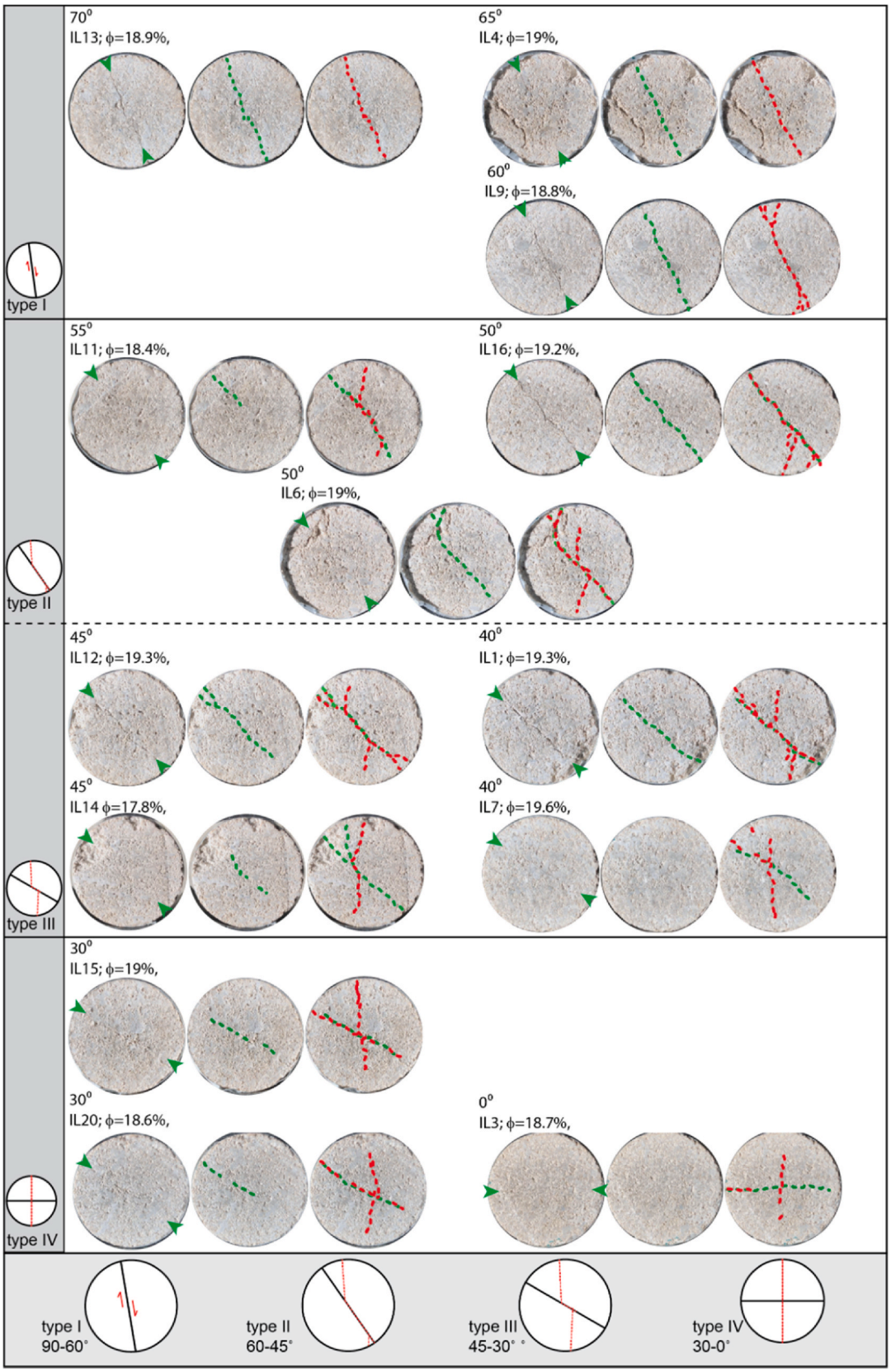

Fig. 7. Indiana limestone, with for each sample left the starting situation with the fracture, in the middle the sample under load, taken before new sliding/fracture is initiated, and on the right the end sample. The green arrows are used to indicate the orientation of the initial crack. The grey box below the main figure contains a summary of the different types of final geometry. For colors, see the digital version of the paper. (For interpretation of the references to color in this figure legend, the reader is referred to the Web version of this article.)

direction of loading. In terms of fracture deflection and coalescence, in this case there is no to very little influence from the initial crack on the orientation of the new crack. Between these two endmember options, the orientation of the initial crack has a decreasing effect on the orientation of the final crack, similar to what would be seen for multi-layer anisotropic samples (Fig. 1). In all cases, the newly formed fracture follows part of the path of the initial crack. We have divided this transition zone in a type II and type III category, with a (somewhat arbitrary) boundary around 45°. In type II samples the newly formed central crack follows the majority of the old diagonal crack, and in type III samples, the newly formed central crack is only slightly deviated by several millimeters.

We can divide the TM samples in two endmembers dependent on their final geometry fracture pattern as well (Fig. 8). Endmember type I are those samples where the initial stylolite is oriented at 90–60°. In these cases, a dense fracture network forms, which surrounds and

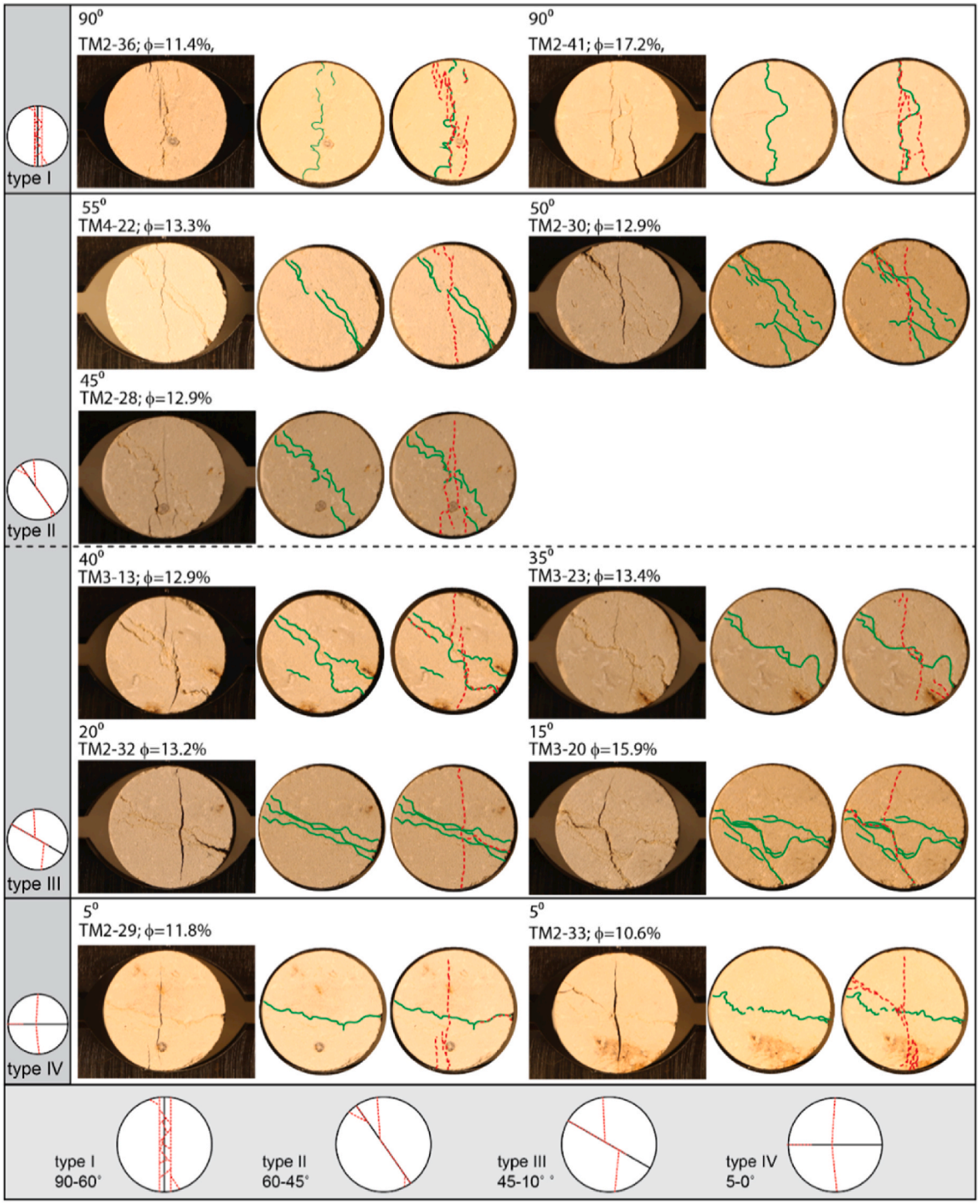

Fig. 8. Final, initial and final geometry including the trace for all Treuchtlinger Marmor samples. Green lines are the original stylolites, red lines the newly formed fractures. For most samples, fracturing occurred during multiple events and the intermediate stages are shown in Fig. 9. The grey box below the main figure contains a summary of the different types of final geometry. (For interpretation of the references to color in this figure legend, the reader is referred to the Web version of this article.)

follows the stylolite. The other endmember, type IV, is for those samples where the initial stylolite is oriented at low angles (5–0°). In these cases, the main new fracture has the "standard" Brazilian disc fracture orientation where the stylolite exerts little influence on the final crack orientation. Type II and type III samples are those in which the final crack follows partly the stylolite orientation, with a gradual transition between mostly the original stylolite orientation to mainly "standard" Brazilian disc orientation. The orientation at which type III transitions to type IV is closer to horizontal than for the IL samples. The final fracture density is a function of orientation, where there are more fractures when the stylolite is oriented at 90°. In all 11 tested stylolite samples there is more than one fracture at the end of the experiment. All samples contain a new central vertical fracture, and in 10 of the 11 cases the stylolite itself visibly opened as well.

For the TM samples, the camera images were of sufficient quality to correlate the movie to the stress-displacement curve, and to analyze the surface deformation with Particle Image Velocimetry. The resulting videos are TM228, TM236, TM241, TM313, TM323, TM422, which are provided as additional material. Note that for the other two stylolite experiments failure occurred within 1 camera frame, hence no video correlation is given. An example of representative PIV analysis for each type, correlated with the stress-displacement curves, are shown in Fig. 9. The expected stress-displacement curve for Brazilian Disc tests is one where the peak stress is reached first, followed by the maximum stress drop. For these experiments however, the stress-displacement curves at high angles show several stress drops as displacement increases. The camera images also show that the sample remains intact after the first stress drop, and in type I samples both the supported stress and stress drop can increase with increasing displacement (see Appendix Fig. A2). In other words, these samples exhibit atypical patterns for Brazilian Disc tests.

For the TM2-36, a 90°/Type I sample, we split the stress-displacement curve in four events (Fig. 9a). In the first and second event, the maximum extensional strain rate occurs in the top bounded by the stylolite zone, and in the middle it occurs symmetrical around the stylolite zone. After the first and second event the top half of the sample shows fractures, as shown by the cartoons in the top left of the stress displacement curve. In the third event, where the stress-displacement curve shows mainly increasing stress with displacement, we see that the top part of the fracture closes, and the fracture extends to the bottom follow the stylolite zone. During the fourth event new fractures initiate throughout the sample, and the extensional zone is partially bounded by the stylolite zone. Due to width of the stylolite zone and the diffuse edges, it is not possible to judge if the fracture gets deflected internally or externally by the stylolite zone.

For TM2-28, a 45°/type III sample, we split the stress-displacement curve in four events (Fig. 9b). In the first event, maximum extensional strain rate occurs throughout the entire sample, and the extensional zone follows partly the boundaries of the stylolite. A fracture initiates in the bottom half of the sample. In the second event, there are small extensional displacement zones outside the stylolite-zones, which mainly leads to opening of the fracture from event 1. During the third event there is both compression and extension throughout the sample, and a new small fracture initiates in the bottom of the sample. During the fourth event, there is a small extensional part around the stylolite in the center, and in the movie a new central fracture appears, though the PIV routine does not have sufficient resolution to pick it up.

For TM3-13, a 40°/type III sample, we split the stress-displacement curve in three events (Fig. 9c). During the first event, the main stress drop, a fracture zone opens and extensional strain rate is present in a zone which is partially bounded by the stylolite in the central and bottom part of the sample. The top left stylolite also opens, but with much lower displacement rates. During the second event the main fractures are active, but with lower strain rates. The strain rates during the third event are one order of magnitude lower, and the fractures are mainly reactivated, showing mainly extension – despite the stress increase with displacement.

For TM2-29, a 5°/type IV sample, we split the stress-displacement curve in two events (Fig. 9d). The first event is the major event, with a large stress-drop (as one would expect for standard Brazilian Disc tests), with extensional strain rates in a narrow band, which is slightly deflected passing the stylolite-zone. During the second step, there is some extension and along both fractures, indicating reactivation.

Overall, in all cases the strain rate is highest symmetrically around the fracture zones during the time they are active. Once the cracks have opened, they can be reactivated, and on occasion slightly close (Fig. 9a). Looking at the magnitudes, the strain rates are higher for the stylolites with an orientation closer to horizontal. The highest strain rate (extension and compression) occurs asymmetrically in the disc, and the orientation of the high strain rate area is affected by the location and orientation of the stylolite. There is no unanimous correlation between the size of the stress drop and the magnitude of the strain rate, though there is an overall pattern of higher strain rates for higher stress drops.

3.3. Finite element model

All models are run for sinusoid stylolite-bearing samples, i.e. for initially cohesive samples, with either an initial contrast in stiffness between the sinusoid and the matrix, or with a change in orientation. The models where initial contrasts in Young's Moduli were set showed stress concentration effects around the contact between host rock and stylolite, especially at the limbs of the sinusoid stylolite zone. This indicates that local tensile stress is higher, which should lead to local crack nucleation when strength is exceeded. Both with a softer (Fig. 10a and b) and a stiffer (Fig. 10d and e) modeled stylolite compared to the matrix the stress concentrations occur, but they switch limb. This illustrates the main qualitative result, which is that a model run without strength contrast (i.e., Young's modulus ratio of 1; Fig. 10c) shows no local stress concentrations, and in all other cases stress concentrations develop. The spatial extent of the variations is controlled by the magnitude of the strength contrast. Rotating the modeled stylolite zone shows similar stress concentrations, where the orientation mildly affects the magnitude and location of the affected area (Fig. 11). Compared to the model without strength contrast, the zone of high stress is more irregular, where irregularity increases with increasing strength contrast (Fig. 10). Irregularity is highest for type II/III orientations, which qualitatively is similar to the results of the PIV analysis (Fig. 9) – though the PIV tracks displacement, and not stress. It should be noted here that these numerical models can only provide qualitative information, as they are based on linear elasticity, i.e. the process of micromechanical failure is not incorporated. Therefore, the absolute values are of limited importance, which is why they are not on the scale.

4. Discussion

Fractures are key in all subsurface engineering projects, since such projects are about keeping fluid where it is (CO_2, H_2 storage) or about ensuring there is sufficient flow so the fluid can be extracted (hydrocarbons, geothermal energy). A better understanding of how pre-existing fractures, veins or stylolites influence formation of new fractures is therefore vital for accurate flow predictions in subsurface engineering projects. We have tested the tensile strength of two different, highly simplified, planar heterogeneities in an otherwise uniform matrix, to determine the effect on mechanical properties and the development of a fracture network. We used two different sample types, with pre-fractured Indiana limestone (interface with zero cohesion), and samples which contained a stylolite (significant cohesion). These highly simplified experiments with a single planar heterogeneity in an otherwise homogeneous matrix are thus a first step to better understanding what happens when a fracture hits a heterogeneity: will it stop, continue, change direction, or bifurcate? In the following, we will first discuss the relative strength of the stylolite compared to the matrix and

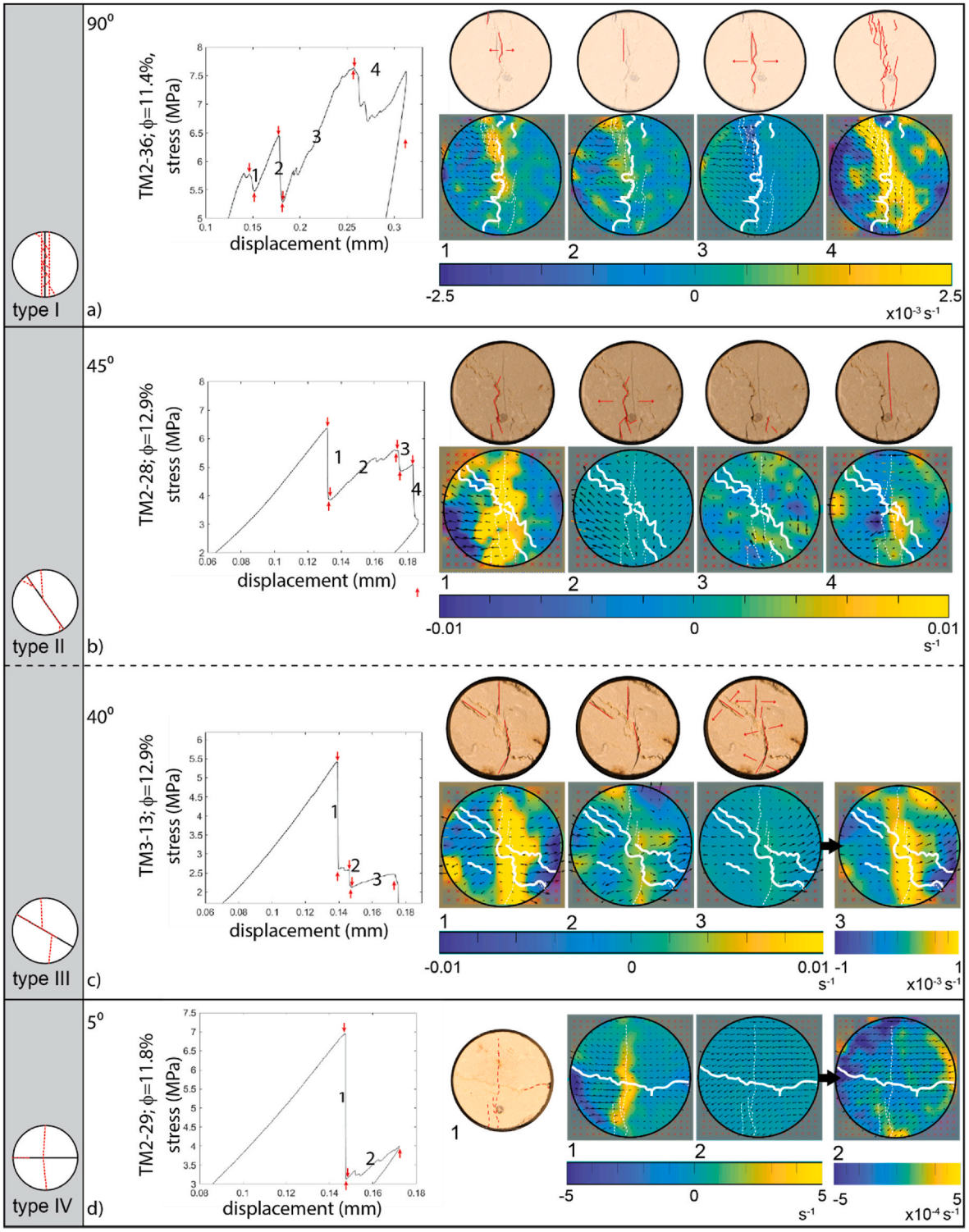

Fig. 9. Stress-displacement curves for representative experiments for each endmember, with the associated particle image velocimetry measurements. In the top left each stress-displacement graph there is a cartoon of which fractures occurred and/or reactivated during each step. The numbers in the graph with the red arrows indicate where the frames are extracted for each graph, where a downward facing arrow is t1, and an upward facing arrow indicates t2. The PIVlab routine is then run on the $image_{t2}$ – $image_{t1}$, leading to the views on the right. The vertical scale has been kept constant, though for TM3-13 and TM2-29 an additional image with blow up of the vertical scale is given (type III and type IV). The first invariant of the compressive strain rate is given, where compression is negative. The final fracture pattern is overlain in white dotted lines, and the initial stylolite geometry in solid white lines. For the other samples the PIVlab Matlab package yielded similar results: a) TM2-36, type I; b) TM2-28, type II; c) TM3-13, type III; d) TM2-29, type IV. (For interpretation of the references to color in this figure legend, the reader is referred to the Web version of this article.)

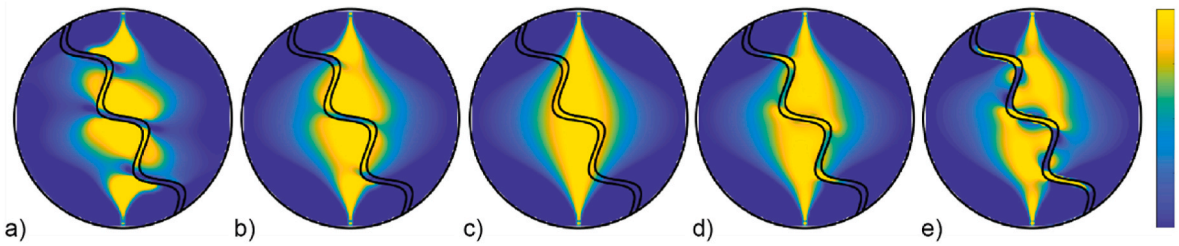

Fig. 10. a)$E_{stylo} = 0.1\ E_{matrix}$; b) $E_{stylo} = 0.5\ E_{matrix}$; $E_{stylo} = E_{matrix}$; $E_{stylo} = 2\ E_{matrix}$; $E_{stylo} = 10\ E_{matrix}$. Qualitative effect of a different ratio in Young's moduli between stylolite and host rock, as modeled with Finite Element models (COMSOL Multiphysics®), for a stylolite positioned at 60°, i.e. type II. The color code (scale on the right) is indicative for local stress in the horizontal direction, where light colors indicate high tensile stress, and dark colors indicate low tensile stress (color scale is the same for all subplots). (For interpretation of the references to color in this figure legend, the reader is referred to the Web version of this article.)

what our results mean for the general effect of a the presence of a planar heterogeneity on the strength and expected fracture pattern in an otherwise intact and uniform rock. We go on to discuss the engineering implications of these results for hydraulic fracture of reservoirs.

4.1. Mechanical nature of the stylolite

Note that, unlike in some previous experimental studies on stylolites,[27,31] we have simply cored the samples as they were, without special care to them retaining in-situ properties. As a consequence, the cohesion of the laboratory sample could be lower than that of the natural sample in-situ, due to damage during sample preparation. However, since the samples remained intact and retained considerable strength, and therefore the mechanical results obtained here are considered useable for the purpose of this study. Note that, even if there would be sample damage due to handling, we would expect some of porosity present in the band to be present in-situ, since there are several places where there is material bridging the gap.

All tested samples with a stylolite were significantly weaker than the samples without a stylolite, regardless of differences in initial porosity (Fig. 6). The nature of the stylolite sample has been investigated with optical microscopy, scanning electron microscopy of the surface, and with micro-tomography. Our tomography data (Fig. 3) indicates that there is a traceable low density zone with the same orientation and tortuosity as the stylolite visible on the sample surface, interpreted to be the same high porosity zone more frequently found surrounding stylolites.[26,27,43] The high porosity zone is also visible in the thin sections, as a discontinuous crack which follows the edge of the low-porosity stylolite zone. The outcrop contains open stylolites and the sample cohesion after coring and the microscopic images indicate that also in-situ this will be a partially open, partially closed crack. In brittle failure in compression, it is shown that the presence of porosity usually leads to weakening.[31,44,45] Likewise, also in Brazilian disc tests the pore space is the weakest path, and therefore porosity contributes to lower strength.[42] However, in these samples, the SEM images also show the presence of the undulating strands, where color and morphology suggest organic material and/or iron oxides, where the microstructure implies some cohesion. In general, stylolites concentrate insoluble material, including hydrocarbons.[22] To summarize, from a mechanical perspective, the stylolite zone consists of an element leading to unknown cohesion (the undulating strands), and an element leading to low cohesion (the open crack with up to tens of micrometer aperture), highlighting the mechanical complexity of these features, even on this centimeter-scale.

In uniaxial tension, discrete element modeling (DEM) of veins inside a matrix has shown that the total weakening and strengthening, as well as the direction of the fracture, depends on the relative strength of the matrix, interface and vein/filler material itself, and also on the direction of the stresses compared to the orientation of the features.[32] These DEM results furthermore indicate that the strength ratio between host rock and vein leads to deflection of the opening crack in most orientations, and that the relative strength contrast leads to either internal deflection (vein weaker than rock) or external deflection (vein stronger than rock). The main difference between the models from Virgo et al. [32] and the current experiments is that in the DEM, the fracture initiated at a notch, whereas in the current set of experiments the stress field is such that the fracture nucleates internally. Though we can clearly see deflection in both the fracture pattern (Fig. 9) in type II and III samples and in the FEM models (Figs. 10 and 11), the width of the stylolite zone is too narrow to indicate with certainty if this is internal or external deflection, and therefore it is not possible to use this as a criterion for relative strength.

The FEM models (Figs. 10 and 11) show that whether the central undulating zone is weaker or stronger than the host rock, the presence of a strength contrast will lead to stress concentrations, and therefore weakening compared to mechanically homogeneous samples. The question is if such weakening would also occur under the presence of a straight fracture, which is partially cemented.[1] López-Buendía et al. looked at different treated and untreated fractured samples under the 90° orientation. They showed that fractured samples are always weaker than intact rock, with in order of decreasing strength: intact rock > cemented stylolite with Fe-ox and clays > cemented stylolite > calcitic vein > partially open stylolite with clays and Fe-ox > open stylolite.[1] Even when applying different resins, samples usually did not recover their full strength. Weakening is in accordance with previously obtained on carbonate samples with a stylolite: in the few studies concerning the mechanical behavior of stylolite-bearing rocks, both in compression[30,31] and in tension[1] stylolite samples were shown to be weaker than stylolite-free samples.

4.2. Mechanical consequences of the presence of a singular planar heterogeneity

The pattern of relative strength as a function of angle in the fractured samples is similar to that reported for layered rocks (e.g. Refs. 4–15), whereas the stylolite-bearing samples show a more isotropic strength. This concurs with a difference in fracture patterns for the end member sample types (type I and IV), see Fig. 12. The mechanics are also different for TM samples than for the fractured Indiana samples. In type I, Indiana limestone exhibits sliding on the existing plane for vertical orientations, whereas Treuchtlinger Marmor shows a complicated fracture network with a vertical orientation, i.e. it is a difference in how much the deformation localizes. For the horizontal orientation, type IV, the Indiana limestone samples exhibited only one new fracture, and the Treuchtlinger Marmor samples exhibited multiple fractures. The horizontal direction for type IV in the stylolite-bearing samples in Fig. 8 is caused by the initial orientation of the stylolite sample, where the stylolite is opened. We interpret this additional complexity in the new structures to be caused by local stress heterogeneities/concentrations along the pre-existing heterogeneities. Note that the veined samples of Mighani et al. [10] also showed easy opening of the veins in the 7 samples tested, even though their samples didn't always have the veins in the optimal orientation for reactivation.

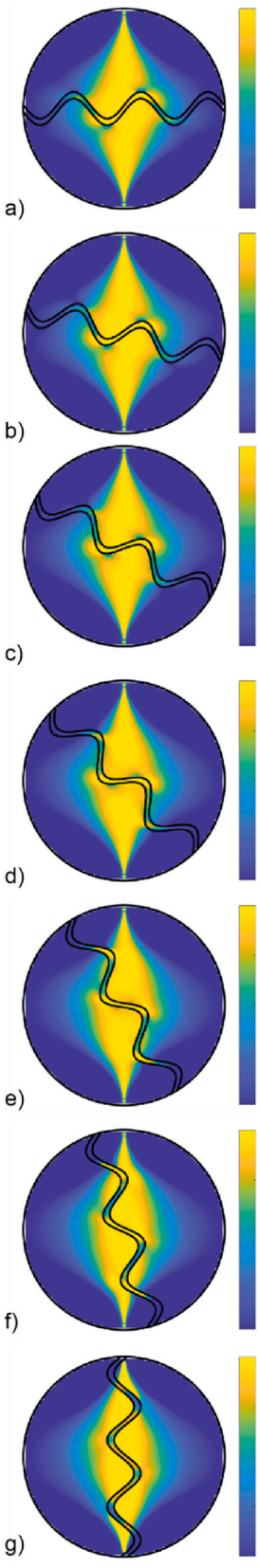

Fig. 11. Qualitative effect of rotation of the stylolite. $E_{stylo} = 2\ E_{matrix}$. a) 0°; b) 15°; c) 30°; d) 45°; e) 60°; f) 75°; g) 90°. Color scale as Fig. 10. (For interpretation of the references to color in this figure legend, the reader is referred to the Web version of this article.)

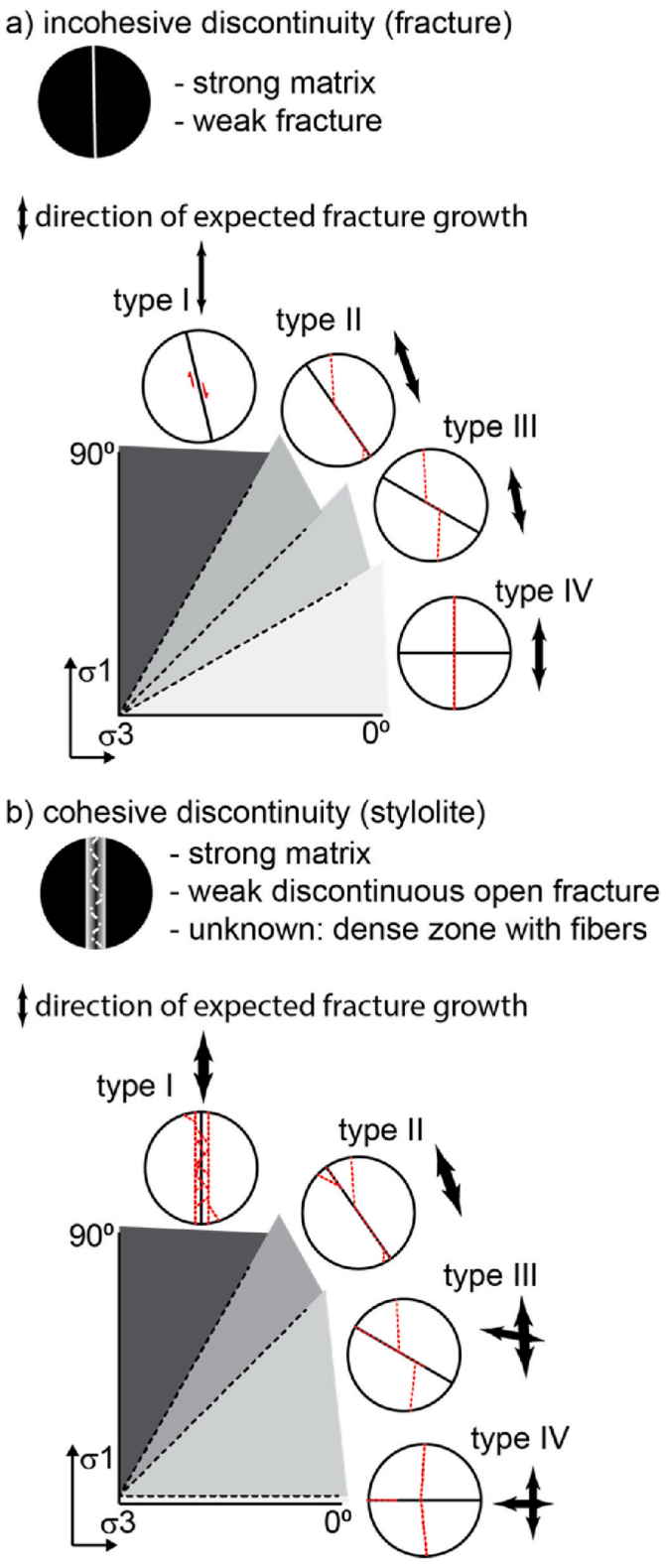

Fig. 12. Schematic summary of the results obtained in this study, and implications for the direction of crack growth, indicated with the black arrows, for a) incohesive (IL) samples and b) stylolite (TM) samples. Permeability enhancement is in the direction of fracture growth, and in/out of the paper (Note: the definitions of fracture angles are in Fig. 2).

It stands to reason that at depth, fractures will have some measure of cohesion, due to fault healing and sealing processes (among many others, see Refs. 46,47). The presence of cohesion across the interface, i.e. the stylolite, significantly changes both anisotropy and fracture pattern (Fig. 12b). Strength is now more or less isotropic, which could be a function of the heterogeneity of the stylolite itself. Each stylolite is composed out of wavy strands of unknown strength and potentially weak porosity, where the CT and pycnometer data indicate that not all porosity is equally distributed throughout the samples. It would be expected that also the strong elements, the insoluble material, is present in varying density throughout the stylolite, and therefore the central part will actually have a different total strength or average strength throughout the samples. Literature shows that veins easily activate at 15° with respect to the loading direction,[10] whereas stylolites activate also when parallel to the loading direction. A stylolite is thus not the same mechanical feature as a vein. However, also when a vein is present, strength is significantly reduced.[10] This confirms our more generic conclusion that the presence of a heterogeneous interface with strength differing from that of the matrix will lead to weakening.

Specifically for stylolites this implies that the presence of a stylolite, as a zone with a different strength, will always weaken a sample, regardless of the properties of the stylolite itself – as long as those properties are different from the host rock. Interestingly, for the thin stylolites tested by Baud et al. [31]; there was no angle-dependent strength, whereas the mm-thickness stylolites in these samples lead to obvious angle-dependent changes in strength. Following our results, another potential explanation for the results from Baud et al. [31] may be that the thin stylolites were too similar in material properties to the host material to constitute a sufficient contrast in mechanical properties, and as a result stress concentration effects were limited.

4.3. Implications for permeability enhancement during hydraulic fracturing

Carbonate reservoirs are often karstified[48] with stylolite seams. Apart from many hydrocarbon fields that are located in carbonates,[16] there are also geothermal reservoirs in Germany (the Munich basin for example, see Ref. 18 and France (the Paris basin for example, see Ref. 17. Moreover, in several countries, including the Netherlands[20] and the United Kingdom,[19] carbonate systems are of interest for fracture plays[49] in geothermal energy. In geothermal plays flow rates are critical to achieving economic success,[50] which is why often fractured and faulted reservoirs are considered.[51] The criticality of achieving sufficient flow rate means that, in particular for deep reservoirs, permeability enhancement is an option to make reservoirs profitable. A well-known method is hydraulic fracture, which involves the opening of mode I cracks. Representative tensile strength for carbonate rocks is thus a critical parameter.

Even though these experiments have been performed at room temperature, our results have implications for permeability enhancement scenarios, which are schematically summarized in Fig. 12. In all cases, the direction of new fracture growth is indicated, though permeability enhancement is mainly in and out of the paper, i.e. parallel to the central axes of the fractures. Considering the effects of orientation on the tensile failure for samples with low to no cohesion (i.e. the IL samples; Fig. 12a), the resulting fracture pattern is similar as found for high and low angles, i.e. the same two end-member categories as[11] (type I and type IV respectively). Type I failure in IL samples is caused by frictional sliding, with limited additional permeability enhancement. Type II and type III failure in IL samples show partial shear and partial tensile failure, with the new fracture (and thus additional permeability) parallel to the main stress direction. Type IV IL samples, i.e. low angles, exhibit renewed tensile failure and full closure of the existing fracture. This means that, when new fractures are formed in fractured samples, the direction of new fracture growth is the only direction of permeability enhancement. The original fracture will actually be partially or even fully closed, so some existing permeability pathways are cut off (Fig. 12a). However, for the stylolite samples, new fractures always open, i.e. permeability is always enhanced regardless of orientation (Fig. 12b). For type I stylolites, an intense new fracture network comes into existence, leading to more significant permeability enhanced than for the no-cohesion samples. In line with the FEM models, we interpret this due to the occurrence of more local and well-distributed stress concentrations along the anastomosing plane. The overall pattern in which direction permeability is enhanced is very similar as for no-cohesion samples, but the stylolite itself is expected to remain an active flow path under all circumstances, due to the local stress concentrations, implying a stronger permeability enhancement when hydrofracturing a formation which contains stylolites.

The presence of boreholes themselves lead to an alteration of the local stress field in the subsurface, with compressive and tensile stresses near the borehole, the location of which depends on the orientation of the maximum and minimum horizontal stress (e.g. Ref. 52). The stylolites tested here are bedding-parallel, which is a first indication these may be sedimentary stylolites (c.f. Ebner et al.[53]). Depending on the relative orientation of the stylolites – and, in the case of sedimentary stylolites, of the bedding – compared to the orientation of the local stress field, the direction and amount of relatively permeability enhancement will differ (schematically shown in Fig. 13). In an extensional environment where σ_1 is vertical the equivalent of type I failure will occur for vertical bedding, type II/III failure will occur for tilted bedding, and type IV will occur failure for horizontal bedding (Fig. 13a). Our results imply there will be some fractures following the stylolite orientations (Fig. 13a, top row), but the majority of the fractures will occur in directions in and out of the paper (Fig. 13a; second row). Type I failure is expected to lead to the most intense fracture network, indicated by thicker and longer fracture lines, and type IV to the least intense fracture network. For a compressive environment with σ_3 vertical, fractures will mainly remain in the horizontal plane as expected for bottom-hole hydrofractures, with minor fracture deviations along the stylolite orientations. These qualitative implications where fracturing of stylolite-bearing targets would be easier could be confirmed by formation integrity tests or leak off tests, which is outside the scope of this paper. When calculating the fracture initiation pressures it has been shown for anisotropic rocks that when the tensile strength displays a strong anisotropy in layered rocks, this cannot be ignored.[15,54,55] Our results imply that a similar conclusion may be drawn for formations with significant stylolite horizons and/or other planar heterogeneities. The significant reduction in tensile strength when heterogeneities are present may explain why observed fracture initiation pressures in extended leak off tests are frequently lower than what would be expected from the tensile strength from mechanical testing from borehole material. Evidently, for practical reasons, any mechanical testing done on core material will be biased towards the competent material, whereas in reality the formation strength is determined by its weakest component.

5. Conclusions

This work shows that the direction of planar heterogeneities, such as stylolites and pre-existing open fractures, can control the direction of the permeable pathways when hydrofracturing a limestone reservoir, barring any effects of the local stress field. The results also indicate that more open fractures will be created when hydrofracturing a stylolite-rich zone in a carbonate formation than when hydrofracturing a zone with open fractures or a homogeneous zone. As long as the material is initially cohesive, finite element shows that the key cause for the formation of several fractures is the presence of undulating heterogeneities with a stiffness contrast. Specifically, we have found the following:

1) Sample strength is always decreased by the presence of a heterogeneity. For a cohesion-less heterogeneity this is clearly anisotropic, with a minimum value when the heterogeneity is parallel to the

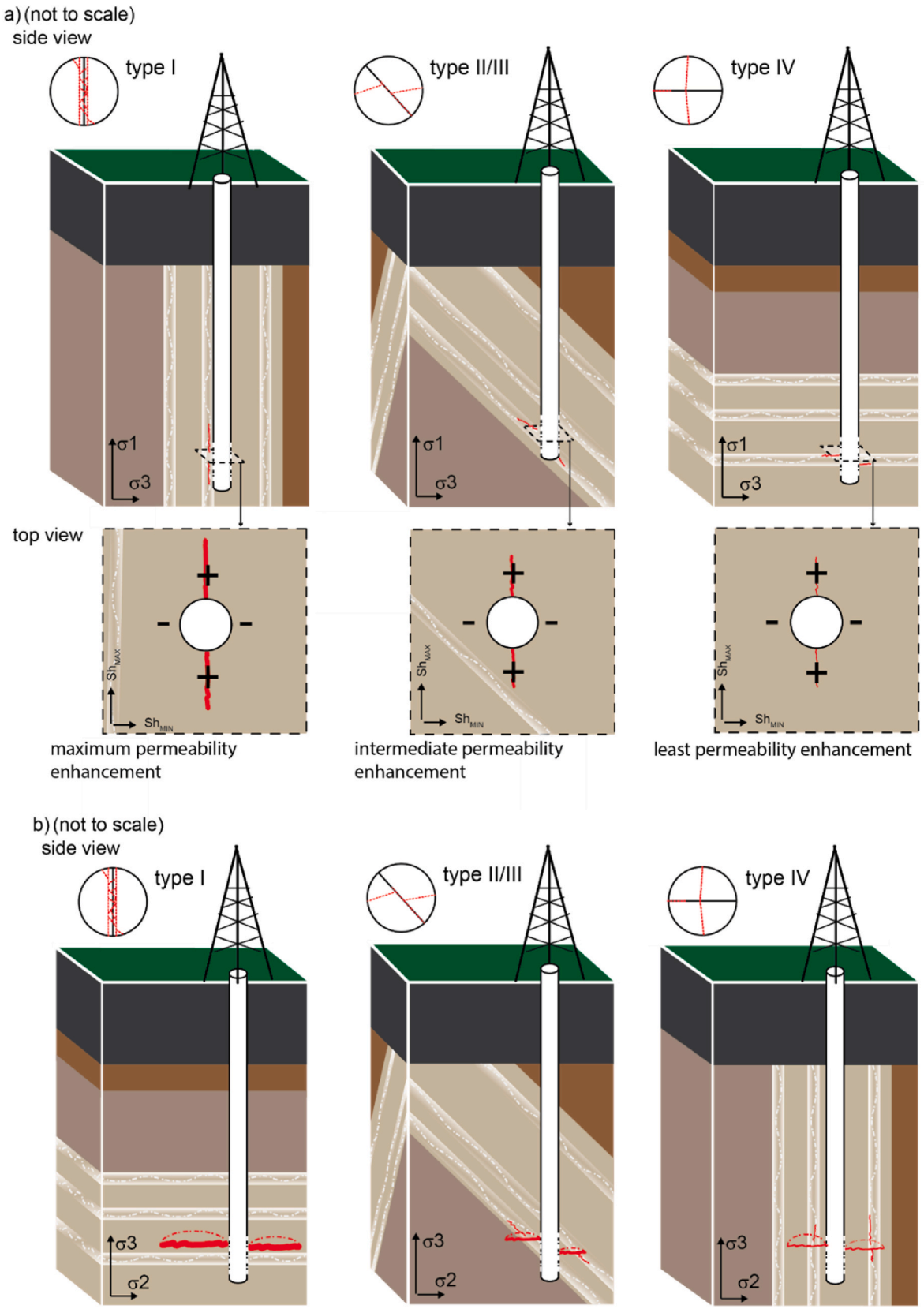

Fig. 13. Schematic representations of implications of hydro-fracturing stylolite-rich formations for different orientations and in different stress regimes. Fracture orientations will be determined by the interplay between the orientations of the principal stresses and the orientation of the stylolites. Fractures indicated in red, with line thickness and length as a qualitative indication of fracture density. Schematics under a) an extensional environment with σ_1 vertical. Some fractures follow the stylolite orientations (top row), but the majority of the fractures will occur in directions in and out of the paper, as indicated by the second row with top view diagrams; and b) a compressive environment with σ_3 vertical. Fractures will mainly remain in the horizontal plane, with minor fracture deviations along the stylolite orientations. (For interpretation of the references to color in this figure legend, the reader is referred to the Web version of this article.)

maximum principal stress, σ_1 (steep angles). For a cohesive heterogeneity, the strength decrease is more isotropic.

2) Depending on the type of heterogeneity, the fracture pattern and resulting permeability enhancement can be divided four categories. The categories are defined depending on the initial orientation of the heterogeneity with respect to the principal stresses, with two clear endmembers, and a more diffusive subdivision in between.

o For a cohesion-less heterogeneity (fracture):

- Steep angles lead to frictional sliding along the interface; and only a small, hypothesized permeability increase.
- Intermediate angles lead to a combination of tensile failure of the matrix and sliding along the interface. The steeper the angle, the more the new fracture follows the path of the existing fracture. The existing fracture is partially closed.
- Shallow angles lead to complete closure of the old fracture and new tensile failure.
- Permeability enhancement is mainly controlled by the direction of new fracture growth.

o For a cohesive heterogeneity of unknown cohesion (such as a stylolite):

- Steep angles lead to intensive failure of the heterogeneous zone, attributed to the presence of stress concentrators, with the potential for a large permeability increase.
- Intermediate angles lead to partial failure along the heterogeneous zone, and the formation of new fractures in the matrix, potentially instigated by mode II failure to accommodate motion.
- Shallow angles lead to the formation of a new fracture plus opening within the heterogeneous zone.
-The stylolite itself is expected to remain an active flow path under all circumstances, implying a stronger and multi-directional permeability enhancement when hydrofracturing a formation which contains stylolites.

Declaration of competing interest

The authors declare that they have no known competing financial interests or personal relationships that could have appeared to influence the work reported in this paper.

Data availability

Data will be made available on request.

Acknowledgments

We would like to thank the technical staff of the Department of Geoscience and Engineering for technical support and Arjan Thijssen at the Microlab for the electron microscopy, all at Delft University of Technology. We thank Guido Blöcher and Detlev Tondeera for providing the Treuchtlinger Marmor samples. In an early stage, this paper greatly benefited from discussions with Ado Farsi. Anne Pluymakers is supported by the Dutch Foundation for Scientific Research (NWO) (grant number: 016.Veni.181.036).

Appendix A. Supplementary data

Supplementary data to this article can be found online at https://doi.org/10.1016/j.ijrmms.2023.105448

Appendix

Table A1
All experiments with either open fracture (Indiana limestone) or stylolite (Treuchtlinger Marmor).

Sample name	porosity (%)	Angle (°)	BtS (MPa)
Indiana limestone			
IL3	18.7	0	2.3
IL15	19	30	2.9
IL20	18.6	30	2.8
IL15	19.3	40	1.6
IL7	19.6	40	2.9
IL12	19.3	45	1.5
IL14	17.8	45	3.1
IL6	19	50	2.0
IL16	19.2	50	0.9
IL11	18.4	55	2.8
IL4	19	65	2.5
IL9	18.8	65	0.4
IL13	18.9	70	0.7
Treuchtlinger Marmor			
TM2-41	17.2	90	3.9
TM2-36	11.4	90	7.6
TM4-22	13.3	70	4.5
TM2-30	13.1	60	6.2
TM2-28	12.9	45	6.3
TM3-13	12.9	60	5.4
TM3-23	13.4	45	3.0
TM2-32	13.2	30	6.5
TM3-20	15.9	30	3.3
TM2-29	11.8	5	7.0
TM2-33	10.6	5	7.5

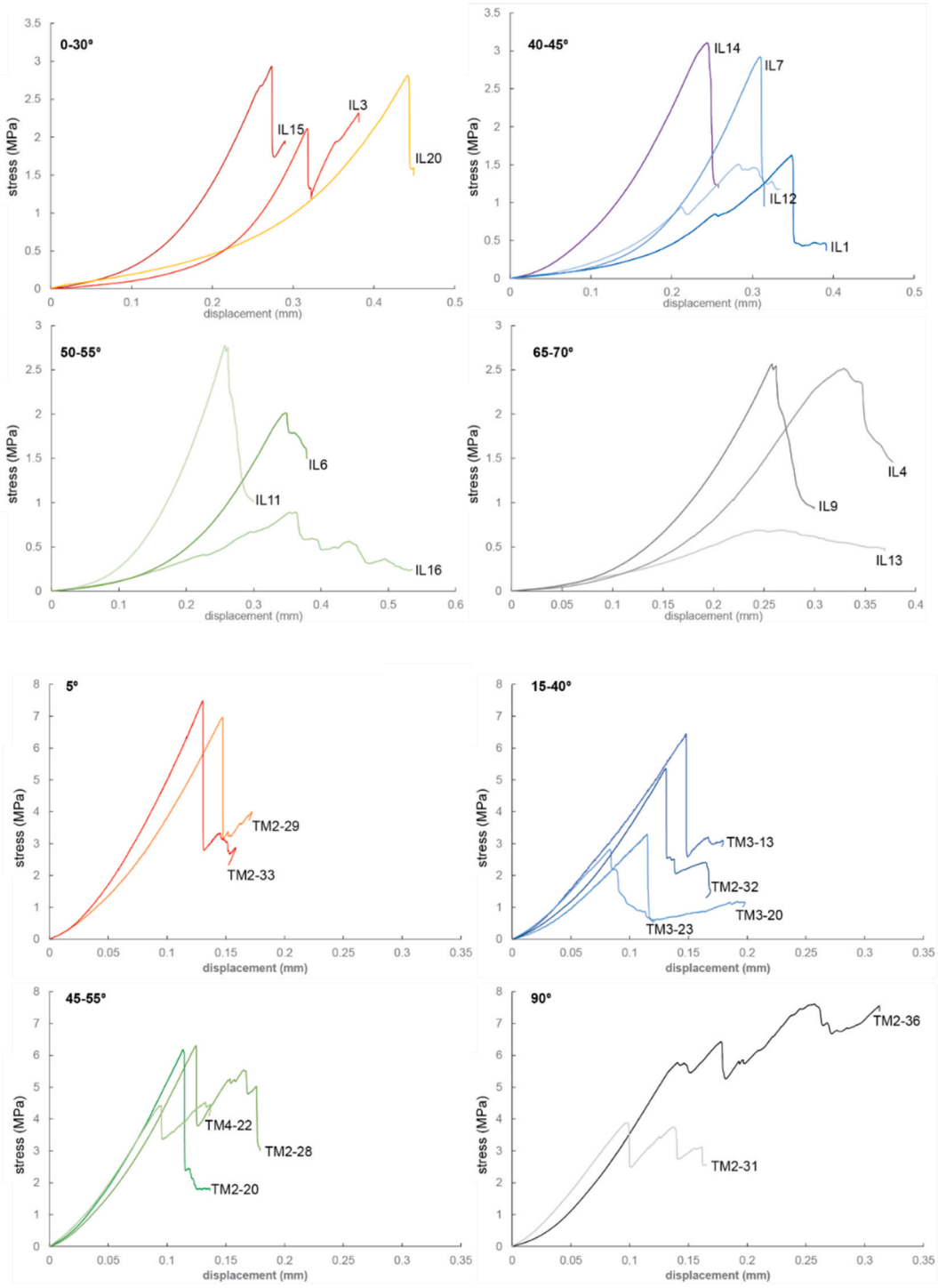

Fig. A1. Stress-displacement curves for all samples. The supported peak stress is the Brazilian test strength (BtS), taken as a proxy for tensile strength. IL stands for Indiana Limestone (open fractures) and TM for Treuchtlinger Marmor (stylolite). The angles for each individual curve are given in the top left corner.

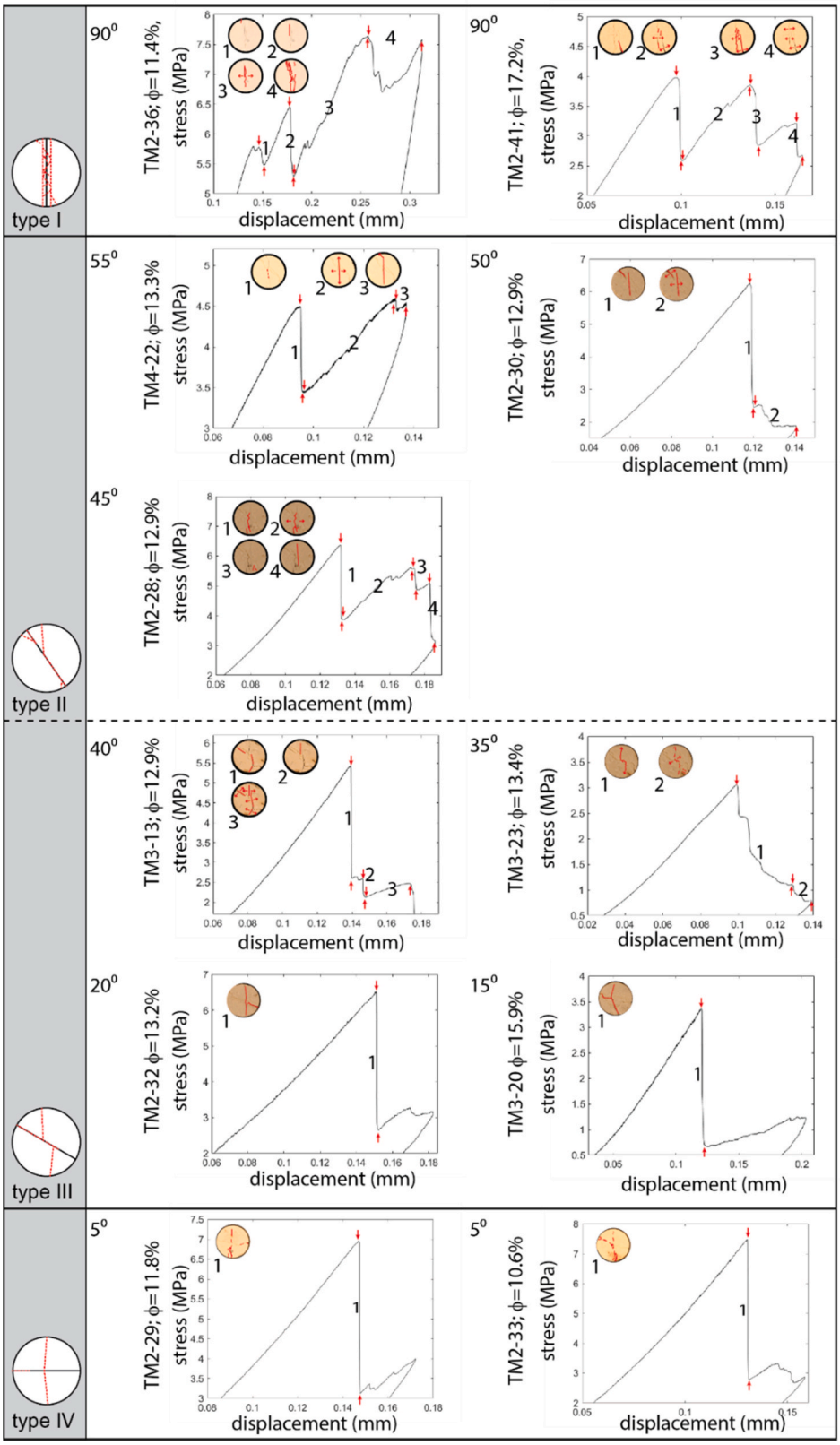

Fig. A2. stress-displacement curves for the stylolite samples categorized per orientation category, where the numbers correlate specific locations of the stress-displacement curve with the camera data.

References

1 López-Buendía AM, Guillem C, Cuevas JM, et al. Natural stone reinforcement of discontinuities with resin for industrial processing. *Eng Geol*. 2013;166:39–51. https://doi.org/10.1016/J.ENGGEO.2013.09.004.

2 Knipe RJ, Jones G, Fisher QJ. Faulting, fault sealing and fluid flow in hydrocarbon reservoirs: an introduction. *Geol Soc Spec Publ*. 1998;147. https://doi.org/10.1144/GSL.SP.1998.147.01.01. vii–xxi.

3 Wang Y, de Hoop S, Voskov D, et al. Modeling of high-enthalpy geothermal projects in fractured reservoirs. In: *World Geothermal Congress, Reykjavik, Iceland*. 2020.

4 Hobbs DW. The tensile strength of rocks. *Int J Rock Mech Min Sci*. 1964;1:385–396. https://doi.org/10.1016/0148-9062(64)90005-1.

5 Chen CS, Pan E, Amadei B. Determination of deformability and tensile strength of anisotropic rock using Brazilian tests. *Int J Rock Mech Min Sci*. 1998;35:43–61. https://doi.org/10.1016/S0148-9062(97)00329-X.

6 Debecker B, Vervoort A. Experimental observation of fracture patterns in layered slate. *Int J Fract*. 2009;159:51–62. https://doi.org/10.1007/s10704-009-9382-z.

7 Tavallali A, Vervoort A. Failure of layered sandstone under Brazilian test conditions: effect of micro-scale parameters on macro-scale behaviour. *Rock Mech Rock Eng*. 2010;43:641–653. https://doi.org/10.1007/s00603-010-0084-7.

8 Dai F, Xia KW. Laboratory measurements of the rate dependence of the fracture toughness anisotropy of Barre granite. *Int J Rock Mech Min Sci*. 2013;60:57–65. https://doi.org/10.1016/j.ijrmms.2012.12.035.

9 Khanlari G, Rafiei B, Abdilor Y. Evaluation of strength anisotropy and failure modes of laminated sandstones. *Arabian J Geosci*. 2015;8:3089–3102. https://doi.org/10.1007/s12517-014-1411-1.

10 Mighani S, Sondergeld Carl H, Chandra SR. Observations of tensile fracturing of anisotropic rocks. In: *SPE Journal*. Society of Petroleum Engineers (SPE); 2016:1289–1301.

11 Ma T, Peng N, Zhu Z, et al. Brazilian tensile strength of anisotropic rocks: review and new insights. *Energies*. 2018;11:304. https://doi.org/10.3390/en11020304.

12 He J, Afolagboye LO. Influence of layer orientation and interlayer bonding force on the mechanical behavior of shale under Brazilian test conditions. *Acta Mech Sin*. 2018;34:349–358. https://doi.org/10.1007/s10409-017-0666-7.

13 Menezes FF, Lempp C. On the structural anisotropy of physical and mechanical properties of a Bunter Sandstone. *J Struct Geol*. 2018;114:196–205. https://doi.org/10.1016/j.jsg.2018.06.010.

14 Abbas HA, Mohamed Z. Anisotropic index strength behaviour and failure mode validation of weathered shale. *Geomechanics Geoengin*. 2020. https://doi.org/10.1080/17486025.2020.1839676.

15 Liu Y, Chen C, Ma T, et al. Experimental investigation on the initiation of hydraulic fractures from a simulated wellbore in laminated shale. *Lithosphere 2021*. 2021. https://doi.org/10.2113/2021/4152918.

16 Ahr WM. *Geology of Carbonate Reservoirs : The Identification, Description and Characterization of Hydrocarbon Reservoirs in Carbonate Rocks*. first ed. Incorporated: John Wiley & Sons; 2008.

17 Regnet JB, David C, Fortin J, et al. Influence of microporosity distribution on the mechanical behavior of oolithic carbonate rocks. *Geomech Energy Environ*. 2015;3:11–23. https://doi.org/10.1016/J.GETE.2015.07.002.

18 Moeck IS, Dussel M, Weber J, et al. Geothermal play typing in Germany, case study Molasse Basin: a modern concept to categorise geothermal resources related to crustal permeability. *Geol en Mijnbouw/Netherlands J Geosci*. 2020;98. https://doi.org/10.1017/njg.2019.12.

19 Busby J. Geothermal energy in sedimentary basins in the UK. *Hydrogeol J*. 2014;22:129–141. https://doi.org/10.1007/s10040-013-1054-4.

20 Boxem T, Veldkamp H, Carpentier S, et al. *Eindrapport Ultra-diepe Geothermie in Nederland* (Utrecht). 2015.

21 Carlson T. *Petrophysical Report of the Dinantian Carbonates in the Dutch Subsurfaceacies Analysis and Diagenetic Evolution of the Dinantian Carbonates in the Dutch Subsurface*. 2019.

22 Toussaint R, Aharonov E, Koehn D, et al. Stylolites: a review. *J Struct Geol*. 2018;114:163–195. https://doi.org/10.1016/J.JSG.2018.05.003.

23 Bruna P-O, Lavenu APC, Matonti C, Bertotti G. Are stylolites fluid-flow efficient features? *J Struct Geol*. 2019;125:270–277. https://doi.org/10.1016/J.JSG.2018.05.018.

24 Vandeginste V, John CM. Diagenetic implications of stylolitization in pelagic carbonates, Canterbury Basin, offshore New Zealand. *J Sediment Res*. 2013;83:226–240. https://doi.org/10.2110/jsr.2013.18.

25 Mehrabi H, Mansouri M, Rahimpour-Bonab H, et al. Chemical compaction features as potential barriers in the permian-triassic reservoirs of south pars field, southern Iran. *J Pet Sci Eng*. 2016;145:95–113. https://doi.org/10.1016/j.petrol.2016.03.020.

26 Ebner M, Piazolo S, Renard F, Koehn D. Stylolite interfaces and surrounding matrix material: nature and role of heterogeneities in roughness and microstructural development. *J Struct Geol*. 2010;32:1070–1084. https://doi.org/10.1016/J.JSG.2010.06.014.

27 Heap M, Reuschlé T, Baud P, et al. The permeability of stylolite-bearing limestone. *J Struct Geol*. 2018;116:81–93. https://doi.org/10.1016/J.JSG.2018.08.007.

28 Larbi JA. Effect of stylolites on the durability of building stones: two case studies. *Heron*. 2003;48:231–247.

29 Pires V, Silva ZSG, Simão JAR, et al. "Bianco di Asiago" limestone pavement – degradation and alteration study. *Construct Build Mater*. 2009;24:686–694. https://doi.org/10.1016/j.conbuildmat.2009.10.040.

30 Rashed MA, Sediek KN. Petrography, diagenesis and geotechnical properties of the El-Rufuf formation (thebes Group), El-Kharga Oasis, Egypt. *J Afr Earth Sci*. 1997;25:407–423. https://doi.org/10.1016/s0899-5362(97)00113-9.

31 Baud P, Rolland A, Heap M, et al. Impact of stylolites on the mechanical strength of limestone. *Tectonophysics*. 2016;690:4–20. https://doi.org/10.1016/J.TECTO.2016.03.004.

32 Virgo S, Abe S, Urai JL. Extension fracture propagation in rocks with veins: insight into the crack-seal process using Discrete Element Method modeling. *J Geophys Res Solid Earth*. 2013;118:5236–5251. https://doi.org/10.1002/2013JB010540.

33 Virgo S, Abe S, Urai JL. The influence of loading conditions on fracture initiation, propagation, and interaction in rocks with veins: results from a comparative Discrete Element Method study. *J Geophys Res Solid Earth*. 2016;121:1730–1738. https://doi.org/10.1002/2016JB012792.

34 Dunham RJ. Classification of carbonate rocks according to depositional textures. In: Ham WE, ed. *Classification of Carbonate Rocks - A Symposium*. AAPG Special Volumes; 1962:108–121.

35 Tamaskovics N, Tondera D, Blöcher G, et al. *Geothermal Research Project "Algäu 2.0" Research Concepts*. Laboratory Investigations and Planning Operations; 2014.

36 Rawling GC, Baud P, Wong T. Dilatancy, brittle strength, and anisotropy of foliated rocks: experimental deformation and micromechanical modeling. *J Geophys Res Solid Earth*. 2002;107. https://doi.org/10.1029/2001jb000472. ETG 8-1-ETG 8-14.

37 Tavallali A, Vervoort A. Behaviour of layered sandstone under Brazilian test conditions: layer orientation and shape effects. *J Rock Mech Geotech Eng*. 2013;5:366–377. https://doi.org/10.1016/J.JRMGE.2013.01.004.

38 Bieniawski ZT, Hawkes I. Suggested methods for determining tensile strength of rock materials. *Int Soc Rock Mech Comm Stand Lab F Tests*. 1978;15:99–103. https://doi.org/10.1016/0148-9062(78)90003-7.

39 Thielicke W, Stamhuis EJ. PIVlab – towards user-friendly, affordable and accurate digital particle image velocimetry in MATLAB. *J Open Res Software*. 2014;2. https://doi.org/10.5334/jors.bl.

40 COMSOL. Structural mechanics module. In: *User's Guide COMSOL*. 2018:1160.

41 Mahabadi OK, Cottrell BE, Grasselli G. *An Example of Realistic Modelling of Rock*. 2010.

42 Chen B, Xiang J, Latham JP, Bakker RR. Grain-scale failure mechanism of porous sandstone: an experimental and numerical FDEM study of the Brazilian Tensile Strength test using CT-Scan microstructure. *Int J Rock Mech Min Sci*. 2020;132,104348. https://doi.org/10.1016/j.ijrmms.2020.104348.

43 Heap MJ, Baud P, Reuschlé T, Meredith PG. Stylolites in limestones: barriers to fluid flow? *Geology*. 2014;42:51–54. https://doi.org/10.1130/G34900.1.

44 Zhu W, Baud P, Wong T. Micromechanics of cataclastic pore collapse in limestone. *J Geophys Res*. 2010;115, B04405. https://doi.org/10.1029/2009JB006610.

45 Baud P, Wong T, Zhu W. Effects of porosity and crack density on the compressive strength of rocks. *Int J Rock Mech Min Sci*. 2014;67:202–211. https://doi.org/10.1016/J.IJRMMS.2013.08.031.

46 Olsen MP, Scholz CH, Léger A. Healing and sealing of a simulated fault gouge under hydrothermal conditions: implications for fault healing. *J Geophys Res*. 1998;103:7421. https://doi.org/10.1029/97JB03402.

47 Renard F, Gratier J-P, Jamtveit B. Kinetics of crack-sealing, intergranular pressure solution, and compaction around active faults. *J Struct Geol*. 2000;22:1395–1407. https://doi.org/10.1016/S0191-8141(00)00064-X.

48 Mazzullo SJ, Chilingarian GV. Chapter 9 Hydrocarbon reservoirs in karsted carbonate rocks. In: *Developments in Petroleum Science*. Elsevier; 1996:797–865.

49 Moeck IS. Catalog of geothermal play types based on geologic controls. *Renew Sustain Energy Rev*. 2014;37:867–882.

50 Daniilidis A, Alpsoy B, Herber R. Impact of technical and economic uncertainties on the economic performance of a deep geothermal heat system. *Renew Energy*. 2017;114:805–816. https://doi.org/10.1016/j.renene.2017.07.090.

51 Daniilidis A, Nick HM, Bruhn DF. Interdependencies between physical, design and operational parameters for direct use geothermal heat in faulted hydrothermal reservoirs. *Geothermics*. 2020;86, 101806. https://doi.org/10.1016/j.geothermics.2020.101806.

52 Aadnoy B, Looyeh R. *Petroleum Rock Mechanics*. Elsevier Inc; 2011.

53 Ebner M, Toussaint R, Schmittbuhl J, et al. Anisotropic scaling of tectonic stylolites: a fossilized signature of the stress field? *J Geophys Res*. 2010;115, B06403. https://doi.org/10.1029/2009JB006649.

54 Ma T, Wu B, Fu J, et al. Fracture pressure prediction for layered formations with anisotropic rock strengths. *J Nat Gas Sci Eng*. 2017;38:485–503. https://doi.org/10.1016/j.jngse.2017.01.002.

55 Ma T, Liu Y, Chen P, et al. Fracture-initiation pressure prediction for transversely isotropic formations. *J Pet Sci Eng*. 2019;176:821–835. https://doi.org/10.1016/j.petrol.2019.01.090.